Experimental realization of quantum algorithms for a linear system inspired by adiabatic quantum computing

Jingwei Wen,[1,*] Xiangyu Kong,[1,*] Shijie Wei,[2] Bixue Wang,[1] Tao Xin,[3,†] and Guilu Long[1,4,5,‡]

[1]*State Key Laboratory of Low-Dimensional Quantum Physics and Department of Physics, Tsinghua University, Beijing 100084, China*

[2]*IBM Research, Beijing 100094, China*

[3]*Shenzhen Institute for Quantum Science and Engineering, Southern University of Science and Technology, Shenzhen 518055, China*

[4]*Tsinghua National Laboratory for Information Science and Technology, Beijing 100084, People's Republic of China*

[5]*Collaborative Innovation Center of Quantum Matter, Beijing 100084, China*

(Received 26 June 2018; published 14 January 2019)

Adiabatic quantum computation is of fundamental importance in the field of quantum computation as it offers an alternative approach to the gate-based model for the manipulation of quantum systems. Recently, an interesting work [arXiv:1805.10549] indicated that we can solve a linear equation system via an algorithm inspired by adiabatic quantum computing. Here we demonstrate the algorithm in a four-qubit nuclear magnetic resonance system by determining the solution of an eight-dimensional linear equation $A\mathbf{x} = \mathbf{b}$. The result is by far the maximum-dimensional linear equation solution with a limited number of qubits in experiments, which include some ingenious simplifications. Our experiment provides the possibility of solving so many practical problems related to linear equations systems and has the potential applications in designing the future quantum algorithms.

DOI: 10.1103/PhysRevA.99.012320

I. INTRODUCTION

Based on the principles of quantum mechanics, quantum computation presents a novel framework to design the efficient algorithms and boost the computation processing with respect to the classical situations. The research on quantum computing can not only bring us powerful ability to manipulate microscopic system, but also can provide us novel perspectives to understand the world and invent new techniques. Since the birth of quantum computation [1,2], so many works have been performed to apply the properties of quantum systems to other research fields, such as communication [3–5], cryptography [6,7], and machine learning [8,9]. Furthermore, many computation models have been put forward including a circuit model [10,11], one-way quantum computing [12], topologic quantum computation [13,14], adiabatic quantum computing (AQC) [15,16] and duality quantum computing [17]. Among them, AQC might be one of the most prospective models for practical application at the recent advances in quantum machine learning because machine learning usually deals with a form of multivariate optimization, which can be directly translated to AQC [18].

In general, AQC starts with a time-dependent initial Hamiltonian H_0, which is convenient to prepare in experiments. By driving the initial Hamiltonian to the target Hamiltonian H_p (the so-called "problem Hamiltonian"), we could get the information encoded in the ground state of H_p [15]. The transition from H_0 to H_p is realized by driving an instantaneous Hamiltonian,

$$H(t) = [1 - s(t)]H_0 + s(t)H_p, \tag{1}$$

where the function $s(t)$ varies from 0 to 1 to parametrize the interpolation. Adiabatic theorem tells us that quantum systems tend to stay in the ground state of the instant Hamiltonian as long as the whole transformation process is sufficiently smooth and slow. Quantum adiabatic evolution can be intrinsically robust against experimental imperfections whereas the necessity of smoothness and long timescales limits its implementation. Recently, some methods have been proposed to optimize the AQC process including randomization method (RM) [19] and shortcut to adiabatic passage [20].

The fundamental algorithm related to quantum machine learning was first proposed by Harrow *et al.* (HHL algorithm) [21]. The HHL algorithm is devoted to preparing a quantum state $|\mathbf{x}\rangle$ representing the solution of a linear system of equation $A\mathbf{x} = \mathbf{b}$. Supposing that A is a $N \times N$ matrix and $\mathbf{b}$ is a N-dimensional vector, the best classical algorithm can find the solution with complexity in $O(N)$ [22], whereas the complexity of the quantum HHL algorithm is polynomial in $\log_2 N$ and κ, where κ is called the condition number, a parameter measuring the numerical instability of A. Recently, it has been shown that the HHL algorithm can be neatly recast in the duality quantum computing formalism where linear combinations of unitary operators are used for computing [17,23]. Experimental realization of the HHL algorithm has been demonstrated the in nuclear magnetic system (NMR) [25], the optical system [24,26], and the superconducting system [27], whereas these experimental protocols only demonstrated the simplest situation of the HHL algorithm by solving a 2×2 linear equation.

*These authors contributed equally to this work.

†xint@sustc.edu.cn

‡gllong@tsinghua.edu.cn

Both the HHL algorithm and its experimental realization are based on a gate model. Recently, an interesting approach has been proposed to implement algorithms inspired by adiabatic quantum computing for solving linear equations. In this paper, we experimentally demonstrate two kinds of algorithms proposed in Ref [28] using the NMR system. On near-term quantum devices, quantum resources will remain scarce and expensive. Thus, this approach shows a significant advantage on the consumption of qubit resources compared with the HHL algorithm. This paper is organized as follows: In Sec. II, we briefly review the basic theory. In Sec. III, experimental setups and experimental procedure will be introduced. Then, we present the experimental results. Finally, a conclusion is given in Sec. IV.

II. A BRIEF REVIEW OF THE THEORY

In this section, we briefly preview the basic framework of quantum algorithms introduced in Ref. [28]. The first quantum algorithm aims at changing the system Hamiltonian from the initial to the final form smoothly, keeping the quantum state staying at the ground state of the instantaneous Hamiltonian,

$$H(s) = A^2(s) - A(s)|\bar{\mathbf{b}}\rangle\langle\bar{\mathbf{b}}|A(s), \tag{2}$$

where $A(s) = (1-s)Z \otimes I + sX \otimes A$ and $|\bar{\mathbf{b}}\rangle = |+, \mathbf{b}\rangle$. The notations X, Y, and Z represent the Pauli matrix, and I is the identity matrix whose dimension is equal to the one of matrix A. State $|\pm\rangle$ are the eigenstates of the Pauli X gate in the computational basis. A lower bound to the spectral gap between the ground-state energy and the energy of the first excited state of $H(s)$ is determined by parameter s ($s \in [0, 1]$): $\Delta^*(s) = (1-s)^2 + (s/\kappa)^2$, and κ is the condition number of the A matrix. Under the natural parametrization, $s(v)$ can be written as

$$s(v) = \frac{\exp\left(v\frac{\sqrt{1+\kappa^2}}{\sqrt{2}\kappa}\right) + 2\kappa^2 - \kappa^2 \exp\left(-v\frac{\sqrt{1+\kappa^2}}{\sqrt{2}\kappa}\right)}{2(1+\kappa^2)}, \tag{3}$$

where $v_a \leqslant v \leqslant v_b$ satisfying

$$v_a = \frac{\sqrt{2}\kappa}{\sqrt{1+\kappa^2}} \log_2(\kappa\sqrt{1+\kappa^2} - \kappa^2), \tag{4}$$

$$v_b = \frac{\sqrt{2}\kappa}{\sqrt{1+\kappa^2}} \log_2(\sqrt{1+\kappa^2} + 1). \tag{5}$$

When parameter v varies from boundary-value v_a to v_b, $s(v)$ will increase progressively from 0 to 1. In this procedure, the eigenstate will correspondingly evolve from $|-, \mathbf{b}\rangle$ to $|+, \mathbf{x}\rangle$, and the target solution state $|\mathbf{x}\rangle$ can be obtained by discarding the ancillary qubit. We choose fixed value $H(v^j)$ of Hamiltonian in the jth step and evolve for a random time t^j with $t^j \in [0, 2\pi/\Delta^*(v^j)]$, which is actually the RM algorithm introduced in Ref. [19].

The second algorithm realizes energy gap amplification and improves the time complexity. In this algorithm, the system Hamiltonian is given by

$$H'(s) = \sigma^+ \otimes A(s)P_{\bar{b}}^{\perp} + \sigma^- P_{\bar{b}}^{\perp} A(s), \tag{6}$$

where $\sigma^{\pm} = (X \pm iY)/2$ and $P_{\bar{b}}^{\perp} = I - |\bar{\mathbf{b}}\rangle\langle\bar{\mathbf{b}}|$ is an orthogonal projector. The eigenvalues of $H'(s)$ are $[0, 0, \pm\sqrt{\gamma_1(s)}, \ldots, \pm\sqrt{\gamma_{2N-1}(s)}]$, where $\gamma_j(s) > 0$ are the nonzero eigenvalues of $H(s)$. When we evolve the system from initial-state $|0\rangle \otimes |-, \mathbf{b}\rangle$, a series of projective measurements on the eigenstates of $H'(s)$ will make the system end up staying in state $|0\rangle \otimes |+, \mathbf{x}\rangle$ with sufficiently high probability. The fixed points we choose can be the same as the ones in the first algorithm, and we evolve the Hamiltonian $H'(v^j)$ for a random time t^j with $t^j \in [0, 2\pi/\sqrt{\Delta^*(v^j)}]$ at the jth step.

Compared with the first algorithm, the second algorithm introduces one more ancillary qubit, whereas the time complexity is decreased from $O[\kappa^2 \log_2(\kappa)/\epsilon]$ to $O[\kappa \log_2(\kappa)/\epsilon]$, where $\epsilon \in (0, 1)$ is a precision parameter. Without the phase estimation procedure, the number of ancillary qubits is independent of the size of the quantum system. Thus, the expansibility of the algorithms can have a much better performance compared with the HHL algorithm in spatial complexity.

III. EXPERIMENTAL SETUPS AND RESULTS

As proof-of-principle demonstrations, we experimentally realize the two algorithms mentioned above by solving eight- and four-dimensional linear equations, respectively. Because of the completeness of the Pauli basis, we can expand matrix A in eight-dimensional Hilbert space. Without the loss of generality, the linear equation we demonstrate in the first algorithm is $A\mathbf{x} = \mathbf{b}$ where matrix $A = (3III + XII - 2XYI + 3XYZ)/4$ and $\mathbf{b} = [1, 1, 1, 1, 1, 1, 1, 1]^T/\sqrt{8}$. It is worth emphasizing that the determination of matrix A and vector $\mathbf{b}$ is arbitrary because this algorithm does not include any subroutines, such as phase estimation which has been used in the HHL algorithm. Moreover, if we set A as a positive-definite matrix, then the parametric matrix can be simplified as $A(s) = (1-s)I + sA$ with $A(s)$ still being a positive-definite nonsingular matrix. As a result, the experimental methods used in this paper should allow for solving even 16×16 linear systems for some special cases.

In experiments, the used four-qubit sample is ^{13}C-labeled transcrotonic acid dissolved in $d6$-acetone with ^{1}H decoupled throughout all the process. The structure and parameters of this molecule are shown in Fig. 1. Notations C1–C4 denote the four qubits, and we choose C1 as the ancillary qubit. The internal Hamiltonian under the weak coupling approximation is

$$H_{\text{int}} = -\sum_{i=1}^{4} \pi \nu_i \sigma_z^i + \sum_{i<j}^{4} \frac{\pi}{2} J_{ij} \sigma_z^i \sigma_z^j, \tag{7}$$

where ν_i is the chemical shift and J_{ij} is the J-coupling strength between the ith and the jth nuclei. All experiments are carried out on a Bruker DRX 400-MHz spectrometer at room temperature (296.5 K).

We start from the thermal equilibrium state and drive the system to the pseudopure state (PPS) using the spatial averaging technique method [29–31]. The procedure is realized by gradient fields and unitary operators which are realized by gradient ascent pulse engineering (GRAPE) [32,33] with the fidelity over 99.5%. The final form of the four-qubit PPS is

$$|\rho_{0000}\rangle = \frac{1-\epsilon}{16} I_{16} + \epsilon |0000\rangle\langle 0000|, \tag{8}$$

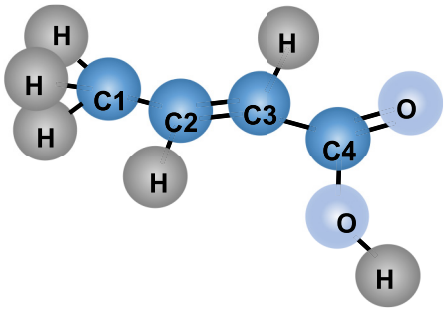

(a)

	C1	C2	C3	C4
C1	1705.5			
C2	41.64	14558.0	*Crotonic Acid*	
C3	1.46	69.72	12330.5	
C4	7.04	1.18	72.36	16764.0
T2	0.84	0.92	0.66	0.79

(b)

FIG. 1. (a) Molecule structure of ^{13}C-labeled crotonic acid. C1–C4 are used as four qubits in the experiment, whereas all ^{1}H's are decoupled throughout the experiment. (b) Molecule parameters of the sample: the chemical shifts and J couplings (in hertz) are listed by the diagonal and off-diagonal elements, respectively. T2's(in seconds) are also shown at the bottom.

where I_{16} represents a 16×16 identity operator and $\epsilon \approx 10^{-5}$ is the polarization. We first apply one X gate on the ancillary qubit followed by four Hadamard gates acting on all qubits, then we finish the preparation of the initial ground-state $|-, \mathbf{b}\rangle$. As we introduced above, the evolution we want to realize is to slowly drive an instant Hamiltonian $H(t)$ which can be equivalently expressed by a unitary evolution $U|-, \mathbf{b}\rangle = |+, \mathbf{x}\rangle$. Practical implementation of AQC is unlikely to perform a smooth sweep but rather to use a piecewise constant Hamiltonian with small jumps between steps. According to the RM theory mentioned above, we divide the total procedure into 300 steps,

$$U = \prod_{i=1}^{300} U_i = U_{300} \cdots U_i \cdots U_2 U_1, \tag{9}$$

where $U_i = e^{-iH(t_i)\Delta_i}$. Notation Δ_i is the random evolution time of the ith step and $\Delta_i \in [0, 2\pi/\Delta^*]$. In our experiment, we pack every 60 steps in one pulse which is also optimized by the GRAPE method, with the length of each pulse 20 ms and the fidelity with theoretical operators over 99%. At the end of the circuit, we obtain the density matrix of the final quantum state by performing quantum-state tomography (QST) [34–38]. QST is finished by applying 17 readout pulses with the duration 0.9 ms after the evolution. Then we can reconstruct all the density-matrix elements of final-state ρ_f.

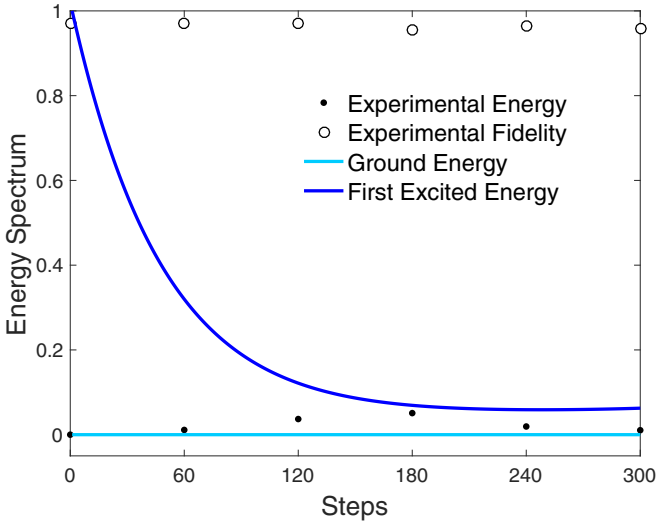

(a)

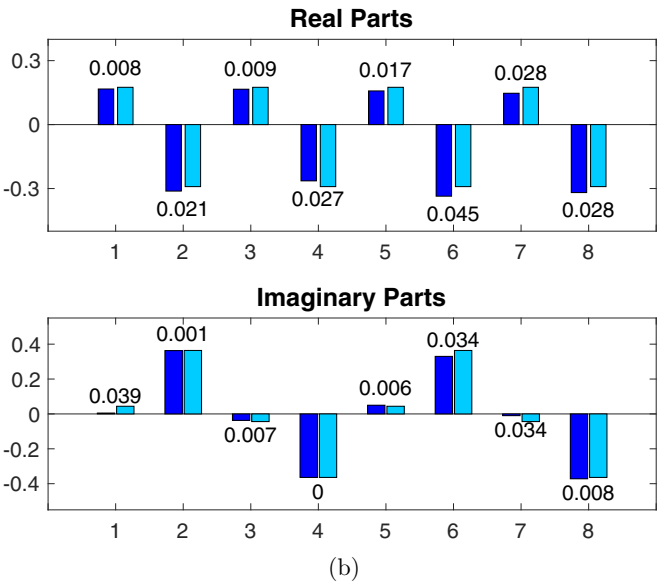

(b)

FIG. 2. Experimental results for the first algorithm. (a) (Energy and fidelity). The light and dark blue solid lines are theoretical values of the first-two energy levels of the time-dependent Hamiltonian, respectively. The solid points (black below) represent the experimental energy results, and the corresponding experimental fidelities are shown by the circle points above. (b) (Final solution). The real and imaginary parts of the theoretical (light blue bars) and experimental (dark blue bars) final quantum states of solution $|\mathbf{x}\rangle$ are shown. The numbers labeled present the corresponding differences between experimental and theoretical values.

We perform four-qubit QST after each step and monitor the energy of system by using definition $\langle H \rangle = \mathrm{tr}(\rho H)$. Experimental results are shown in Fig. 2(a) . It is shown that the ground energy of the system does not exceed the energy of the first excited state within the range of experimental error, which means the process we realized is definitely adiabatic. Using the definition $F(\rho, \sigma) = \mathrm{tr}(\rho\sigma)/\sqrt{\mathrm{tr}\,\rho^2}\sqrt{\mathrm{tr}\,\sigma^2}$ [39], the fidelity between the theoretical and the experimental measured quantum state is over 95.5% in the whole process of the experiment. After tracing out the ancillary qubit, we find that

the fidelity between the experimental three-qubit quantum-state ρ_x and the theoretical solution $|\mathbf{x}\rangle\langle\mathbf{x}|$ is about 98.4%. We reconstruct the quantum state from the final density matrix and find the solution x_{exp} in experiment (theoretical solution x_{th}), which is also shown in Fig. 2(b). We also label the difference values between the experimental and the theoretical data beside the bars in the picture.

By far, we have demonstrated the experimental realization of the first algorithm. In the following we would turn to the discussion of the second algorithm and its experimental results. In this case, we attempt to solve a four-dimensional linear equation where matrix A and vector $\mathbf{b}$ are chosen as $A = (3II + 2ZI + 3XI - 3XY)/4$ and $\mathbf{b} = [1, 1, 1, 1]^T/2$.

The experimental setups are almost the same: Total numbers of the evolution steps we set are 300, and we pack every 60 steps in one package and optimize them with the GRAPE method. The four-qubit fidelities in experiments are all over 97%. After tracing out the ancillary qubits (C1 and C2), the two-qubit density matrix representing the solution is created and the two-qubit fidelities are about 97.65% on average. As a result, the experimental solution $x_{\text{exp}} = [0.157 - 0.039i, 0.193 + 0.009i, 0.454 - 0.590i, 0.509 + 0.352i]$, and the theoretical solution is $x_{\text{th}} = [0.175 - 0.019i, 0.175 + 0.019i, 0.500 - 0.468i, 0.500 + 0.468i]$. We also list the energy levels of the experimental and theoretical states in Fig. 3. The results indicate that the second algorithm does amplify the energy gap and the energy drift is merely 5% of the energy gap between the ground-state energy level and the closest excited energy level. Therefore, the second algorithm obtains better adiabatic performance than the first one with an identical evolution time, which means the second algorithm is more robust in the AQC model.

The inaccuracies of our experiments are mostly eliminated because of the robustness of the adiabatic evolution. However, if the amplitude and phase of the control field have random fluctuations with a range of 5 Hz and 5°, which is common in the actual experimental process, the adiabatic passage will still have a random variation. We numerically analyzed the fluctuation range of the energy and fidelities after each step of the adiabatic passage and list the theoretical range in Table I. The actual experimental results are also listed in the table for comparison.

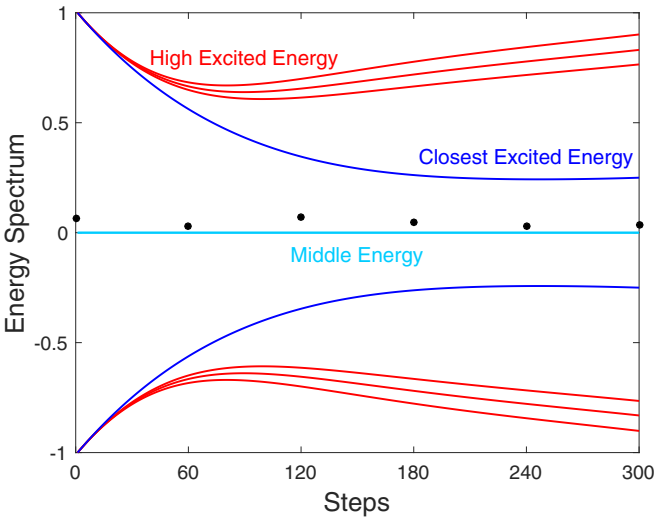

FIG. 3. Experimental results for the second algorithm. The solid lines are theoretical values of the energy spectrum of the time-dependent Hamiltonian. The light blue line is the middle level of the spectrum, and the other lines represent the closest eight energy levels. The black points represent experimental energy results in each step of our experiment.

IV. CONCLUSION

To summarize, we first demonstrate the solution of an eight-dimensional linear equation system by utilizing algorithms inspired by adiabatic quantum computing in our NMR platform. The experimental results match well with the theoretical expectations, and we also compare the performance of the two different algorithms. This is a solution of the largest-dimensional linear equations realized in a quantum simulator. It is worth emphasizing that these algorithms have better expansibility than the previous algorithms. The determinations of matrix A and vector $\mathbf{b}$ are arbitrary, and the complicated subroutines, such as phase estimation and variable-time amplitude amplification are not necessary. In the future, one of the predominant challenges is how to establish a scalable physical system for quantum computation, and resources of qubits are still very precious in the present development stage of quantum information. Under such a

TABLE I. Error range of the two algorithms based on the assumption that the fluctuations of amplitude and phase are within a range of 5 Hz and 5°. We numerically analyzed the fluctuations of the energy and fidelities after each step and list the fluctuation range. The actual experimental results are also listed in the table for comparison.

	Algorithm 1				Algorithm 2	
	Energy		Fidelity		Energy	
Error range	Theory range	Experiment	Theory range (%)	Experiment (%)	Theory range	Experiment
Step 1	0.0002–0.0029	0.0010	96.70–99.98	97.00	0.0000–0.1080	0.0657
Step 2	0.0020–0.0129	0.0112	96.79–99.18	96.98	0.0018–0.0422	0.0298
Step 3	0.0067–0.0437	0.0369	96.79–98.82	96.97	0.0035–0.1090	0.0689
Step 4	0.0100–0.0673	0.0509	95.22–97.06	95.59	0.0048–0.0940	0.0489
Step 5	0.0089–0.0420	0.0193	95.82–97.30	96.30	0.0064–0.0601	0.0290
Step 6	0.0072–0.0412	0.0105	94.33–96.99	95.70	0.0072–0.1050	0.0370

background, the protocols we demonstrate would be scalable and meaningful because the number of required ancillary qubits is independent of the size of the quantum system. In experiments, we realize the demonstration of these algorithms by solving eight- and four-dimensional linear equations with high fidelities. It is believed that the process we demonstrated can be extended to other quantum computing platforms.

ACKNOWLEDGMENTS

This work was supported by the National Basic Research Program of China under Grants No. 2017YFA0303700 and No. 2015CB921001 and the National Natural Science Foundation of China under Grants No. 61726801, No. 11474168, and No. 11474181.

[1] R. P. Feynman, Int. J. Theor. Phys. **21**, 467 (1982).
[2] P. Benioff, J. Stat. Phys. **22**, 563 (1980).
[3] P. W. Shor and J. Preskill, Phys. Rev. Lett. **85**, 441 (2000).
[4] F. G. Deng, G. L. Long, and X. S. Liu, Phys. Rev. A **68**, 042317 (2003).
[5] F. G. Deng and G. L. Long, Phys. Rev. A **69**, 052319 (2004).
[6] A. K. Ekert, Phys. Rev. Lett. **67**, 661 (1991).
[7] C. H. Bennett, Phys. Rev. Lett. **68**, 3121 (1992).
[8] P. Rebentrost, M. Mohseni, and S. Lloyd, Phys. Rev. Lett. **113**, 130503 (2014).
[9] Z. Li, X. Liu, N. Xu, and J. Du, Phys. Rev. Lett. **114**, 140504 (2015).
[10] D. Deutsch, Proc. R. Soc. London, Ser. A **425**, 73 (1989).
[11] A. C. Yao, in *Proceedings of the 34th Annual Symposium on Foundations of Computer Science* (IEEE Computer Society, New York, 1993), pp. 352–361.
[12] R. Raussendorf and H. J. Briegel, Phys. Rev. Lett. **86**, 5188 (2001).
[13] A. Y. Kitaev, Ann. Phys. **303**, 2 (2003).
[14] Z. Luo, J. Li, and Z. Li, Nat. Phys. **14**, 160 (2018).
[15] E. Farhi, J. Goldstone, and S. Gutmann, arXiv:quant-ph/0007071.
[16] X. Peng, Z. Liao, N. Xu, G. Qin, X. Zhou, D. Suter, and J. Du, Phys. Rev. Lett. **101**, 220405 (2008).
[17] G. L. Long, Commun. Theor. Phys. **45**, 825 (2006).
[18] P. Wittek, *Quantum Machine Learning: What Quantum Computing Means to Data Mining* (Academic, San Diego, 2014).
[19] S. Boixo, E. Knill, and R. D. Somma, Quantum Inf. Comput. **9**, 0833 (2009).
[20] X. Chen, I. Lizuain, A. Ruschhaupt, D. Guéry-Odelin, and J. G. Muga, Phys. Rev. Lett. **105**, 123003 (2010).
[21] A. W. Harrow, A. Hassidim, and S. Lloyd, Phys. Rev. Lett. **103**, 150502 (2009).
[22] Y. Saad, *Iterative Methods for Sparse Linear Systems* (Society for Industrial and Applied Mathematics, Philadelphia, 2003).
[23] S. J. Wei, T. Wang, D. Ruan, and G. L. Long, Sci. Sin. **47**, 1277 (2017).
[24] J. Pan, Y. Cao, X. Yao, Z. Li, C. Ju, H. Chen, X. Peng, S. Kais, and J. Du, Phys. Rev. A **89**, 022313 (2014).
[25] X.-D. Cai, C. Weedbrook, Z.-E. Su, M.-C. Chen, M. Gu, M.-J. Zhu, L. Li, N.-L. Liu, C.-Y. Lu, and J.-W. Pan, Phys. Rev. Lett. **110**, 230501 (2013).
[26] S. Barz, I. Kassal, and M. Ringbauer, Sci. Rep. **4**, 6115 (2014).
[27] Y. Zheng, C. Song, M.-C. Chen, B. Xia, W. Liu, Q. Guo, L. Zhang, D. Xu, H. Deng, K. Huang, Y. Wu, Z. Yan, D. Zheng, L. Lu, J.-W. Pan, H. Wang, C.-Y. Lu, and X. Zhu, Phys. Rev. Lett. **118**, 210504 (2017).
[28] Y. Subasi, R. D. Somma, and D. Orsucci, arXiv:1805.10549.
[29] D. G. Cory, M. D. Price, and T. F. Havel, Physica D **120**, 82 (1998).
[30] S. Y. Hou, Y. B. Sheng, and G. R. Feng, Sci. Rep. **4**, 6857 (2014).
[31] H. Li, X. Gao, and T. Xin, Sci. Bull. **62**, 497 (2017).
[32] N. Khaneja, T. Reiss, and C. Kehlet, J. Magn. Reson. **172**, 296 (2005).
[33] C. A. Ryan, C. Negrevergne, M. Laforest, E. Knill, and R. Laflamme, Phys. Rev. A **78**, 012328 (2008).
[34] J.-S. Lee, Phys. Lett. A **305**, 349 (2002).
[35] G. Feng, G. Xu, and G. Long, Phys. Rev. Lett. **110**, 190501 (2013).
[36] G. M. Leskowitz and L. J. Mueller, Phys. Rev. A **69**, 052302 (2004).
[37] G. Feng, G. L. Long, and R. Laflamme, Phys. Rev. A **88**, 022305 (2013).
[38] J. Li, S. Huang, Z. Luo, K. Li, D. Lu, and B. Zeng, Phys. Rev. A **96**, 032307 (2017).
[39] E. Fortunato, M. Pravia, N. Boulant, G. Teklemariam, T. Havel, and D. Cory, J. Chem. Phys. **116**, 7599 (2002).